Universität Karlsruhe (TH)
Forschungsuniversität • gegründet 1825

Institut für Mechanik

Large Deformation Frictional Contact Formulation for Low Order “Solid-Shell” Elements

Alexander Konyukhov, Karl Schweizerhof, Matthias Harnau
Universität Karlsruhe, Institut für Mechanik

Institut für Mechanik
Kaiserstr. 12, Geb. 20.30
76128 Karlsruhe
Tel.: +49 (0) 721/ 608-2071
Fax: +49 (0) 721/ 608-7990
E-Mail: ifm@uni-karlsruhe.de
www.ifm.uni-karlsruhe.de

Large Deformation Frictional Contact Formulation for Low Order "Solid-Shell" Elements

Alexander Konyukhov, Karl Schweizerhof and Matthias Harnau

2004

Keywords
Contact problem, Friction, Covariant Formulation, Velocity Description, Integration with Subdomains.

Abstract
A special contact formulation which is compatible with the so-called 'Solid-Shell' is developed for applications involving large deformation and frictional contact. The contact conditions are considered in the covariant form from the surface geometry point of view, which is very similar to shell theory. The contact integral and the necessary kinematical values are considered on the tangent plane of the contact surface for which a special surface coordinate system is introduced. A focus is on the regularization of the frictional conditions, which leads to evolutions equations in the form of covariant derivatives. A geometrical interpretation of these equations as the parallel translation is used to overcome the problem of discontinuity of the characteristics on element boundaries. The main advantage of the developments is a more algorithmic and geometrical structure of the tangent matrix.

Different integration techniques based on higher order integration formulae as well as based on the subdivision of the contact area into subdomains allow to construct elements with diminishing error for the contact patch test in the non-frictional case. The segment-to-segment and the segment-to-analytical surface approaches are developed for the frictional problems with large sliding. Within the numerical examples the focus is also on the effect where a 3D continuum approach as e.g. for the solid-shell elements appears to be beneficial in the context with frictional contact.

1 INTRODUCTION

Frictional contact is a specific interaction between bodies contacting each other along surfaces, therefore, the change of these surfaces in the covariant form can be described by differential geometry. An essential feature to model frictional contact problems is the formulation of the contact conditions as kinematical constraints which leads to a nonlinear problem and, therefore, within the correct description of the solution process, to a consistent linearization problem. The development of the finite element description for the frictional problem is documented in the following references: [1], [2], [3], [4]. A series of publications are devoted to the development of the so-called smooth contact conditions, see [4], [5], [6].

In this contribution we propose a fully covariant description of contact which can be applied for arbitrary smooth surfaces. The contact conditions are considered in a specially defined spatial local coordinate system including the well-known closest point procedure. This coordinate system is chosen on the surface of the so-called "solid-shell" elements, described in details in [7] and [8]. All differential operations necessary for kinematics and linearization are considered as covariant derivatives. Special attention is on the consideration of the operations and the weak form on the tangent plane. The constitutive equations for the tangential tractions within the penalty regularization, named here as the evolution equations, are considered in the covariant description as a parallel translation on the contact surface. It is important to use this form of the constitutive equations, because the consistent linearization of the contact integral together

with these equations leads to the correct symmetrical form of a tangent matrix in the case of sticking. We have to note that an artificial non-symmetry of the tangent matrix in 3D was mentioned in Laursen and Simo [2]. In order to overcome this e.g. Wriggers proposed in [10] the regularization of the stick conditions based on a functional used in mesh tying procedures. In the current contribution the geometrical interpretation of the parallel translation allows also to develop an integration scheme for the tangential tractions and to overcome the problem of the discontinuity of the history variables at element boundaries, which was also discussed e.g. in Krstulovic-Opara et. al. [5] and Puso and Laursen [6].

The introduction of the local coordinate system allows also to treat the case of contact with rigid surfaces, which is often used in metal-forming problems. The projection procedure in this case is then turned into the definition of the penetration directly from the surface equation.

The integration of the contact integral leads to a problem of integrating a discontinuous integrand, therefore, the integration with subdomains as an example for an adaptive technique is proposed to improve the results for the patch test. For further investigations a series of contact elements including a different approach for the evaluation of the contact integral is considered to check the effect of the numerical integration more closely. Finally, after demonstrating the effect of various integration schemes on some simple examples, a sheet metal forming example with rather industrial content is taken to demonstrate various characteristics within this process.

2 GEOMETRY AND KINEMATICS OF CONTACT

We consider two interacting bodies (Figure 1) which are coming in contact, if a "slave" point **S** of the second surface penetrates into the "master" surface. Penetration is defined as the shortest distance between the two surfaces of the contacting bodies.

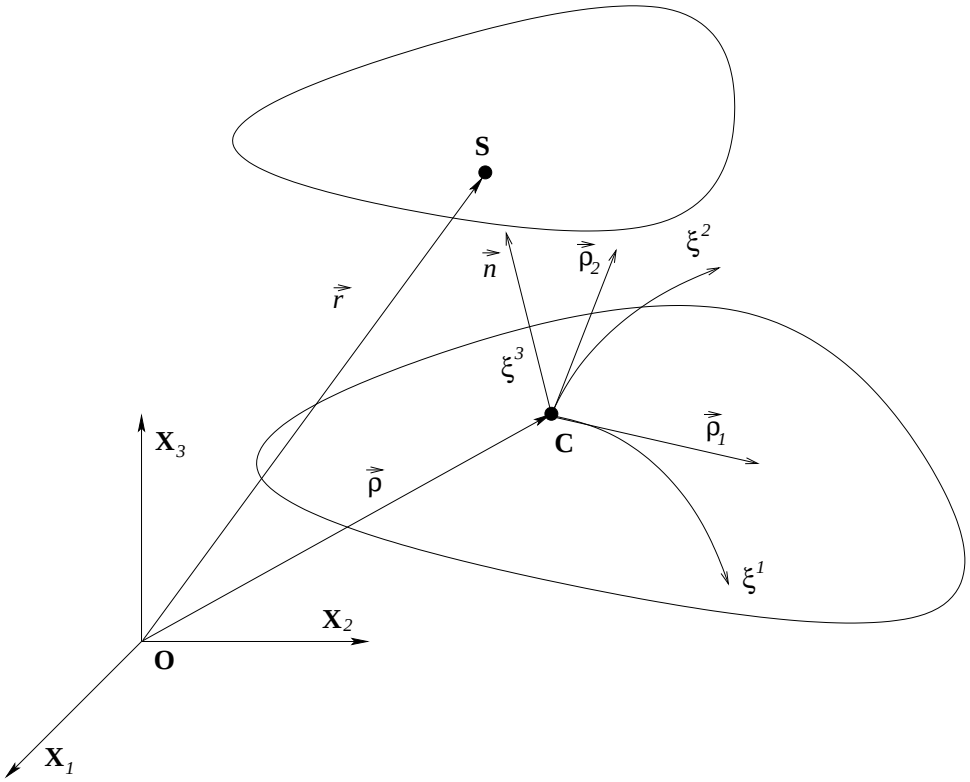

Figure 1: Two body contact. Local surface coordinate system on master surface.

As contact between two bodies is dominantly an interaction between these two surfaces, the

main aim of the following consideration is to take advantage of the differential geometry of the contact surfaces in order to describe the kinematics of the contact conditions.

2.1 Spatial coordinate system

Assuming the projection procedure to be computed, we define the "slave" point **S** via the following equation

$$\vec{r}(\xi^1, \xi^2, \xi^3) = \vec{\rho} + \xi^3 \vec{n}, \tag{1}$$

where $\vec{\rho}$ is a vector of the penetration point C on the "master" surface, $\vec{n}$ is the surface normal. Eqn. (1) defines a 3D coordinate system. A value of the penetration g, essential for formulating the non-penetration conditions in contact mechanics, is exactly the third coordinate in our surface coordinate system:

$$\xi^3 = g = (\vec{r}_s - \vec{\rho}) \cdot \vec{n}. \tag{2}$$

The equilibrium equations for contact will now be formulated in the defined local coordinate system, and since contact is an interaction between surfaces, each necessary equation especially for the linearization will be considered on the tangent plane, i.e. at $\xi^3 = 0$. For this, we define all the geometrical and differential characteristics with special attention on their values on the tangent plane.

The base vectors of the coordinate system are given as

$$\vec{r}_i = \frac{\partial \vec{r}}{\partial \xi^i} = \vec{\rho}_i + \xi^3 \vec{n}_i = (a_i^k - \xi^3 h_i^k)\vec{\rho}_k, \quad i = 1, 2, \quad \vec{r}_3 = \vec{n}, \tag{3}$$

where the a_i^k terms are components of the metric tensor and the h_i^k terms are components of the curvature tensor. The covariant components of the metric tensor of the spatial coordinate system are defined via the dot product of the vectors given in eqn. (3).

$$g_{ij} = (\vec{r}_i \cdot \vec{r}_j) = a_{ij} - 2\,\xi^3 h_{ij} + (\xi^3)^2 h_{ik} h_j^k, \quad i = 1, 2 \quad g_{i3} = 0, \quad g_{33} = 1. \tag{4}$$

2.2 Differential characteristics

Two important kinematical characteristic quantities are the convective velocities of the "slave" point and the full time derivative of a vector in the tangent plane.

Taking a full time derivative of eqn. (1) we obtain:

$$\frac{d}{dt}\vec{r}_s(t, \xi^1, \xi^2, \xi^3) = \frac{\partial \vec{\rho}}{\partial t} + \frac{\partial \vec{\rho}}{\partial \xi^j}\dot{\xi}^j + \frac{\partial \vec{n}}{\partial t}\xi^3 + \vec{n}\dot{\xi}^3 + \frac{\partial \vec{n}}{\partial \xi^j}\dot{\xi}^j. \tag{5}$$

Convective velocities $\dot{\xi}^i$ are obtained after evaluating the dot product of the full time derivative (5) and of the base vectors in (3). After some algebraic operations they get the following form:

$$\dot{\xi}^3 = \dot{g} = (\vec{v}_s - \vec{v}) \cdot \vec{n}, \tag{6}$$

and

$$\dot{\xi}^j = \hat{a}^{ij} \left[(\vec{v}_s - \vec{v}) \cdot \vec{\rho}_i - \xi^3 \left(\frac{\partial \vec{n}}{\partial t} \cdot \vec{\rho}_i + h_i^k (\vec{v}_s - \vec{v}) \cdot \vec{\rho}_k \right) \right], \tag{7}$$

where $\hat{a}^{ij}$ are components of the inverse matrix $[a_{ij} - 2\xi^3 h_{ij} + (\xi^3)^2 h_i^k h_{jk}]$.

Assuming that the value of the penetration g remains always small, each characteristic quantity is considered on the tangent plane. This is a main feature of the velocity description which leads to a simple form of the tangent matrix and an efficient application to non-frictional problems, see Konyukhov and Schweizerhof [9]. Thus, having taken $\xi^3 = 0$, we obtain the values of the convective velocities (7) on the tangent plane as

$$\dot{\xi}^j = a^{ij}(\vec{v}_s - \vec{v}) \cdot \vec{\rho}_i. \tag{8}$$

The full time derivative of an arbitrary vector $\vec{T}$ in the spatial coordinate system computed in convective coordinates ξ^1, ξ^2, ξ^3 via covariant derivatives is a frame indifferent derivative and coincides with the Lie time derivative $\mathcal{L}_t$ defined in the form

$$\mathcal{L}_t \vec{T} := \mathbf{F} \frac{d}{dt}(\mathbf{F}^{-1}\vec{T}) = \frac{d}{dt}\vec{T} \tag{9}$$

where $\mathbf{F}$ is a push-forward and $\mathbf{F}^{-1}$ a pull-back operator. The Lie time derivative is a standard mathematical tool for the linearization, therefore, the computation of the covariant derivatives will be employed for further linearization. Let $\vec{T}$ be now the vector of tangential tractions in the tangent plane in covariant components, i.e.

$$\vec{T} = T_i \vec{r}^{\,i}|_{\xi^3=0} = T_i \vec{\rho}^{\,i}. \tag{10}$$

Its full time derivative is computed employing the covariant derivatives

$$\frac{dT_i}{dt} = \frac{\partial T_i}{\partial t} + \left(\frac{\partial T_i}{\partial \xi^j} - \Gamma^k_{ij} T_k \right) \dot{\xi}^j + h^k_i T_k \dot{\xi}^3, \tag{11}$$

where Γ^k_{ij} are surface Christoffel symbols.

3 WEAK FORMULATION IN THE SPATIAL COORDINATE SYSTEM

Now we consider the contact tractions $\vec{T}_1$ and $\vec{T}_2$ on both contact surfaces s_1 and s_2 in the current configuration. Assuming $\delta\vec{u}_i$ as a variation of the displacement field on the surface s_i and equilibrium at the contact boundary $\vec{T}_1 ds_1 = -\vec{T}_2 ds_2$, the work of the contact forces is determined in the following integral

$$\delta W_c = \int_{s_1} \vec{T}_1 \cdot (\delta\vec{u}_1 - \delta\vec{u}_2) ds_1. \tag{12}$$

The integral in (12) is considered in the local coordinate system, therefore, up to this point one surface was specified as master surface and the other as slave surface. With s_1 as slave surface, the previous notation is now slightly redefined:

- $\vec{u}_1 = \vec{r}_s$ is a slave point;
- $\vec{u}_2 = \vec{\rho}$ is a projection of the slave point onto the master surface;

the traction vector in the local coordinate system becomes then:

$$\vec{T}_1 = \vec{T} = N\vec{n} + T_i \vec{\rho}^{\,i}. \tag{13}$$

Using the kinematical dependencies from eqn. (5) and decomposing the contact force as in eqn. (13), the contact integral is cast into the following form:

$$\delta W_c = \int_s N \delta\xi^3 ds + \int_s [T_i \delta\xi^i + \xi^3 T_i (\delta\vec{n} \cdot \vec{\rho}^{\,i} - h^i_j \delta\xi^j)] ds. \tag{14}$$

The full integral must be considered with the variation of the convective coordinates for which from eqn. (6) the penetration is obtained as the third coordinate $g = \xi^3$ in the form

$$\delta\xi^3 = \delta g = (\delta\vec{r}_s - \delta\vec{\rho}) \cdot \vec{n}, \tag{15}$$

and from eqn. (7) the convective coordinate ξ^j are found in the form

$$\delta\xi^j = \hat{a}^{ij}\left[(\delta\vec{r}_s - \delta\vec{\rho})\cdot\vec{\rho}_i - \xi^3\left(\delta\vec{n}\cdot\vec{\rho}_i + h_i^k(\delta\vec{r}_s - \delta\vec{\rho})\cdot\vec{\rho}_k\right)\right]. \tag{16}$$

The full formulation with eqns. (14), (15), (16) in the local coordinate system is very cumbersome. However, as the value of penetration g must be small during the solution, which is an important feature of the current velocity description, we consider the full contact integral only on the tangent plane, i.e. $\xi^3 = 0$. Thus, the following form remains:

$$\delta W_c = \int_s N\delta g ds + \int_s T_j\delta\xi^j ds = \tag{17}$$

$$= \int_s N(\delta\vec{r}_s - \delta\vec{\rho})\cdot\vec{n}ds + \int_s T_j a^{ij}(\delta\vec{r}_s - \delta\vec{\rho})\cdot\vec{\rho}_i ds,$$

which is accompanied by the variation of the convective coordinates on the tangent plane in the form:

$$\delta\xi^j = a^{ij}(\delta\vec{r}_s - \delta\vec{\rho})\cdot\vec{\rho}_i. \tag{18}$$

It must be noted that the formulation of the contact integral in the form presented in eqn. (17) is mostly used in contact mechanics, see e.g. Wriggers [10] and Laursen [11].

4 REGULARIZATION AND LINEARIZATION

We will use the standard regularization technique as described e.g. in Wriggers [10] and Laursen [11], which is based on an elasto-plastic analogy to model Coulomb friction.

The normal traction N is represented by the penalty method as

$$N = \epsilon_N\langle g\rangle, \tag{19}$$

where ϵ_N is a penalty parameter and $\langle\rangle$ are Macauley brackets.

For the regularization of the tangential contact traction we propose a rate equation based on usage of the covariant derivatives, see eqn. (11), in the following form:

$$\frac{dT_i}{dt} = (-\epsilon_T a_{ij} + \Gamma_{ij}^k T_k)\dot{\xi}^j - h_i^k T_k\dot{\xi}^3 \tag{20}$$

The system of ordinary differential equations for the computation of the tangential traction (20) is taken as *the evolution equations*, which are important for the linearization process. Using the form with the covariant derivatives (20) leads to a symmetrical tangent matrix for sticking. Based on the geometrical interpretation of the covariant derivative as a parallel translation the following equation for trial covariant components $(T^{tr})_i^{(n+1)}$ of the tangential traction vector is obtained

$$(T^{tr})_i^{(n+1)} = T_k^{(n)} a_{(n)}^{kj}\ (\vec{\rho}_j^{\,(n)}\cdot\vec{\rho}_i^{\,(n+1)}) - \epsilon_T\Delta\xi^k a_{ik}^{(n+1)} \tag{21}$$

where $\Delta\xi^k$ is defined as

$$\Delta\xi^k = \begin{cases} (\Delta\vec{\rho}\cdot\vec{\rho}_j)\ a_{(n+1)}^{kj} & \textit{for segment-to-segment (STS) and} \\ & \textit{node-to-segment (NTS) approaches, with} \\ & \Delta\vec{\rho} = (\vec{\rho}_{C^{(n)}} + \vec{u}_{C^{(n)}})\,|_{\xi^1_{(n)},\,\xi^2_{(n)}} - \vec{\rho}_{C^{(n+1)}}|_{\xi^1_{(n+1)},\,\xi^2_{(n+1)}} \\ (\vec{u}\cdot\vec{\rho}_j)a_{(n+1)}^{kj} & \textit{for segment-to-analytical surface (STAS) approach} \end{cases} \tag{22}$$

where $\xi^i_{(n+1)}$ and $\xi^i_{(n)}$ are convective coordinates of the projection point $\vec{\rho}_C$ at the load step $(n+1)$ and (n) respectively; and $\vec{u}_{C^{(n)}}$ is the incremental displacement vector of the projection point.

Afterwards, the return mapping in the standard form, Wriggers [10] and Laursen [11], is applied.

4.1 Linearization

The contact integral in eqn. (17) is computed over the "slave" surface, which is defined by a set of "slave" points. Each parameter in the contact integral is considered in the spatial local coordinate system of the "master" surface, i.e. as a function of the convective coordinates ξ^i. Therefore, the linearization of the "slave" surface element ds will not enter the linearization process. Thus ds is assumed to remain constant within the linearization.

The idea behind the forthcoming linearization is the application of the covariant derivatives consequently to the normal part of the contact integral and to each part of the return-mapping algorithm together with the evolution equations (20) and considering their values on the tangent plane. This is a quite cumbersome process for which we only present the final result.

The normal part of the contact integral (17) has the following form:

$$\delta W_c^N = \int_s \epsilon_N \langle g \rangle \delta g ds = \int_s \epsilon_N \langle (\vec{r}_s - \vec{\rho}) \cdot \vec{n} \rangle \ (\delta \vec{r}_s - \delta \vec{\rho}) \cdot \vec{n} ds. \tag{23}$$

The linearization of eqn. (23) leads to:

$$D(\delta W_c^N) =$$

$$= \int_S \epsilon_N \ H(-g) \ (\delta \vec{r}_s - \delta \vec{\rho}) \cdot (\vec{n} \otimes \vec{n})(\vec{v}_s - \vec{v}) dS - \tag{24}$$

$$- \int_S \epsilon_N \ H(-g) \ g \ \left(\delta \vec{\rho}_{,j} \cdot a^{ij} (\vec{n} \otimes \vec{\rho}_i)(\vec{v}_s - \vec{v}) + (\delta \vec{r}_s - \delta \vec{\rho}) \cdot a^{ij} (\vec{\rho}_j \otimes \vec{n}) \vec{v}_{,i} \right) dS - \tag{25}$$

$$- \int_S \epsilon_N \ H(-g) \ g \ (\delta \vec{r}_s - \delta \vec{\rho}) \cdot h^{ij} (\vec{\rho}_i \otimes \vec{\rho}_j)(\vec{v}_s - \vec{v}) dS. \tag{26}$$

For the details of the linearization of the normal part δW_c^N and the application to the non-frictional problems we refer to Konyukhov and Schweizerhof [9].

The tangential part of the contact integral (17) has the following general form:

$$\delta W_c^T = \int_s T_j a^{ij} (\delta \vec{r}_s - \delta \vec{\rho}) \cdot \vec{\rho}_i ds, \tag{27}$$

Restricting us here to the sticking case only, the linearized functional becomes

$$D_v(\delta W_c^T) =$$

$$- \varepsilon_T \int_s (\delta \vec{r}_s - \delta \vec{\rho}) a^{ij} \vec{\rho}_i \otimes \vec{\rho}_j (\vec{v}_s - \vec{v}) ds \tag{28}$$

$$- \int_s T_i \left((\delta \vec{r}_s - \delta \vec{\rho}) \ a^{il} a^{jk} \ \vec{\rho}_k \otimes \vec{\rho}_l \ \vec{v}_j + \delta \vec{\rho}_{,j} \ a^{ik} a^{jl} \ \vec{\rho}_k \otimes \vec{\rho}_l \ (\vec{v}_s - \vec{v}) \right) ds \tag{29}$$

$$+ \int_s T_i h^{ij} (\delta \vec{r}_s - \delta \vec{\rho}) \cdot (\vec{\rho}_j \otimes \vec{n} + \vec{n} \otimes \vec{\rho}_j) (\vec{v}_s - \vec{v}) ds. \tag{30}$$

As sticking is a conservative problem a symmetric form is found.

For efficiency considerations it is an interesting issue that the contact tangent matrix can be subdivided into three parts: the "main" or "constitutive" part eqn. (24) and (28), the "rotational" part (25) and (29) and the "curvature" part (26) and (30). The "main" part contains a tensor product of surface coordinate vectors: these are the normal $\vec{n}$ and the surface base vectors $\vec{\rho}_i$ for normal and tangential parts of the tangent matrix respectively and represent stiffnesses in both directions. The "rotational" part contains derivatives of $\delta\vec{\rho}$ and $\vec{v}$ with respect to the convective coordinates ξ^j and, therefore, represents the rotation of a contact surface during the incremental solution procedure. The "curvature" part contains components of the curvature tensor h^{ij} and, therefore, represents the change of the curvature of the master surface.

5 COMPUTATION OF THE CONTACT INTEGRAL

Within the finite element method the contact integral in eqn. (17), leading to the residual, as well as the integrals in the linearized equations leading to the consistent tangent matrix, have to be computed using one or another quadrature formulae. In the most common approach known as "node-to-surface" (NTS) technique the value at the nodes from the finite element discretization of the "slave" part is taken directly. As it is known, this technique can be only directly applied in the case of linear approximations for both "slave" and "master" parts, see [1], and it does not satisfy the patch test, see [13]. This fact can be explained as under-integration of the contact integral, because the Lobbatto quadrature formula with only two integration points gives exactly a nodal collocation formula in this case. As an improvement different quadrature formulae of higher order can be used. Then the question arrises: how many integration points have to be taken in order to achieve a certain error bound? The usual formula to estimate the integration error does not give the correct answer, because it requires the differentiability of the integrand up to the certain order. However, this is not the case for the computation of the contact integral, which is discussed in the following: The function in the integral is defined on the master element, but the computation of the integral has to be done over the unknown slave surface. In practice, the penetration of "slave" points, e.g. integration points, from different "slave" segments into the master segment is checked. This can be considered as integration of auxiliary functions over the known master surface which again define a function which is discontinuous on the master surface. The a-priori error estimation in the case of the application of Gauss quadrature rules for discontinuous functions is a more complicated question, because it is necessary to know the behavior of the integrand, see e.g. [12]. However, this is in general not known in the considered cases of rather arbitrary contact surfaces. One can only expect, that increasing the number of integration points leads to a reduction of the integration error. As an alternative an adaptive technique to decrease the integration error a subdivision of the integration area into subdomains together with lower order integration in each subdomain is suggested, see e.g. [12]. This leads to a considerable improvement of the characteristics for the patch test.

6 CONTACT WITH RIGID SURFACES DESCRIBED BY ANALYTICAL FUNCTIONS

If a body contacts a rigid surface, the latter one is chosen as a "slave" surface in our description, but the integration will be done over the "master" surface. The rigid surface is then parameterized by internal coordinates α^1, α^2. Then a point $\vec{r}_s$ of this surface has to satisfy eqn. (1) as a point in the local coordinate system of the contact element too. This condition leads to the following equation

$$\vec{r}_s(\alpha^1, \alpha^2) = \vec{\rho}(\xi^1, \xi^2) + \xi^3 \vec{n}. \tag{31}$$

The "slave" point projection procedure, which was necessary for the previous description with surface segments, now turns into the determination of the surface point defined by equation (31). Using a "segment-to-segment" (STS) type strategy for the computation of the contact integral, first integration points ξ_I^1, ξ_J^2 are defined on the "master" segment and then the corresponding internal coordinates α^1, α^2 of the rigid surface as well as the penetration ξ^3 are computed e. g. by the Newton method. For this algorithm we define a function $F(\alpha^1, \alpha^2, \xi^3)$ with the components given in eqn. (31)

$$\mathbf{F} = \begin{bmatrix} x_{s1} - x_1 - n_1\xi^3 \\ x_{s2} - x_2 - n_2\xi^3 \\ x_{s3} - x_3 - n_3\xi^3 \end{bmatrix} \quad \text{with} \quad x_i = x_i(\xi^1, \xi^2). \tag{32}$$

Its derivative with respect to the coordinates $(\alpha^1, \alpha^2, \xi^3)$ is:

$$\mathbf{F}' = \begin{bmatrix} x_{s1,1} & x_{s1,2} & -n_1 \\ x_{s2,1} & x_{s2,2} & -n_2 \\ x_{s3,1} & x_{s3,2} & -n_3 \end{bmatrix}. \tag{33}$$

Then, the Newton iteration procedure reads as follows for iteration step n:

$$\Delta\boldsymbol{\alpha}_n = \begin{bmatrix} \Delta\alpha_n^1 \\ \Delta\alpha_n^2 \\ \Delta\xi_n^3 \end{bmatrix} = -(\mathbf{F}')_n^{-1}\ \mathbf{F}_n, \tag{34}$$

$$\boldsymbol{\alpha}_{n+1} = \boldsymbol{\alpha}_n + \Delta\boldsymbol{\alpha}_n.$$

For some analytical surfaces, the solution of eqn. (34) is simplified. Surfaces of revolution and cylindrical surfaces are among them. Some simple surfaces, such as plane surface, cylinder, sphere and torus even allow to define the value of the penetration directly.

We consider surfaces of revolution, defined by curve $f(r)$ uniquely projected onto the r axis, see Fig. 2. The revolution of the curve about axis OZ gives a surface of revolution. In a Cartesian coordinate system it can be written as

$$\mathbf{r}_s(r, \phi) = \begin{bmatrix} x_s \\ y_s \\ z_s \end{bmatrix} = \begin{bmatrix} r\cos\phi \\ r\sin\phi \\ f(r) \end{bmatrix}. \tag{35}$$

Then the iteration vector $\Delta\boldsymbol{\alpha}_n$ in eqn. (34) gets the following form:

$$\Delta\boldsymbol{\alpha}_n = \begin{bmatrix} \Delta r_n \\ \Delta\phi_n \\ \Delta\xi_n^3 \end{bmatrix} \tag{36}$$

with

$$\Delta r_n = \frac{1}{D} \cdot ((x_3 - f(r))(n_1\cos\phi + n_2\sin\phi) + n_3(r - x_1\cos\phi - x_2\sin\phi))$$

$$\Delta\phi_n = \frac{1}{r \cdot D} \cdot ((f(r) - x_3 - rf'(r))(n_1\sin\phi - n_2\cos\phi) + f'(r)(n_1x_2 - n_2x_1)$$
$$+n_3(x_1\sin\phi - x_2\cos\phi))$$

$$\Delta\xi_n^3 = \frac{1}{r \cdot D} \cdot \big(f'(r)(x_1\cos\phi + x_2\sin\phi - r) + f(r) - x_3 + \xi^3[f'(r)(n_1\cos\phi + n_2\sin\phi) - n_3]\big)$$

with

$$D = -n_3 + f'(r)(n_1\cos\phi + n_2\sin\phi).$$

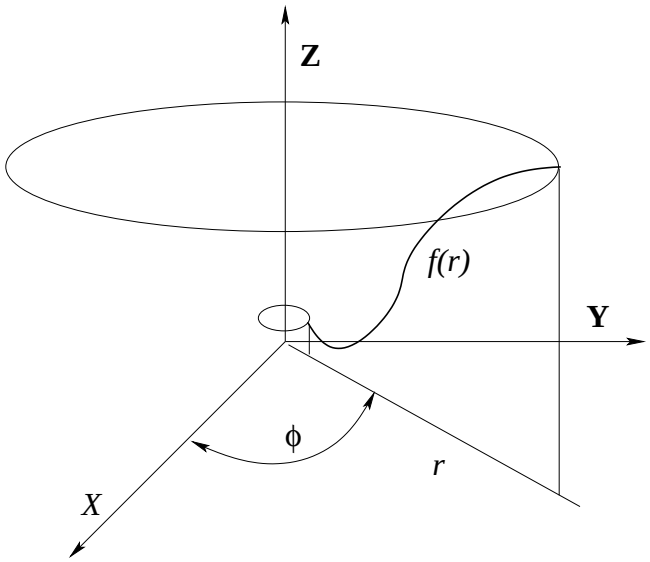

Figure 2: Surface of revolution as an analytical contact surface.

7 NUMERICAL EXAMPLES

7.1 Patch test. Non-frictional case.

Here we consider the application of the segment-to-segment contact approach with various integration schemes to the modified patch test problem without friction, originally proposed in Crisfield [13] for the 2D patch test. The upper block has dimensions $1 \times 1 \times 0.5$ and it is meshed with a regular rectangular mesh $3 \times 3 \times 2$. The lower block has the same geometry as the upper block, and has a finer, but distorted mesh $6 \times 6 \times 2$, see Fig. 3. Both blocks are made of elastic material with the following parameters: Youngs modulus $E = 1.0 \cdot 10^5$, Poisson ratio $\nu = 0.3$. The value of the penalty is chosen as $\varepsilon = 1.0 \cdot 10^7$. During contact the upper block is considered as a slave. An uniform vertical displacement of $\Delta = 0.05$ is applied on the top surface.

The integration algorithm based on integration of subdomains is an approximate approach to integrate discontinuous functions. Here we show, that with this technique it is possible to construct a sequence of results with diminishing error to finally satisfy the patch test. In order to investigate the normal contact traction N for uniform stresses, the normal stress σ_z and the vertical nodal displacement u_z of the contact surface of the lower block are chosen. Their values are controlled by the mean value $\bar{x}$, while the standard deviation σ and the coefficient of variation $C_v = 100\% \cdot \sigma/\bar{x}$ are computed to estimate the variation. In table 1 the results concerning the mean value and the coefficient of variation for the following quantities are given: sum of contact tractions $N = \varepsilon_p g_N$ over the surface, computed at Gauss points of the contact surface; normal stresses σ_z, computed for the upper and lower surface of each element of the lower block; nodal vertical displacements u_z for the contact surface. For comparison, the first computation was made for the node-to-surface approach with a reduced penalty value of 10^5 due to the convergence problems in this case. As is known, this approach fails the patch test and, as expected, leads here to the maximum of the coefficient of variation.

From table 1 it becomes clear that the integration with subdomains leads to smaller variations than an algorithm with standard Gauss integration. It appears rather remarkable for this application that the variations of the tractions remain constant while the variation of the stresses and displacements falls below one percent.

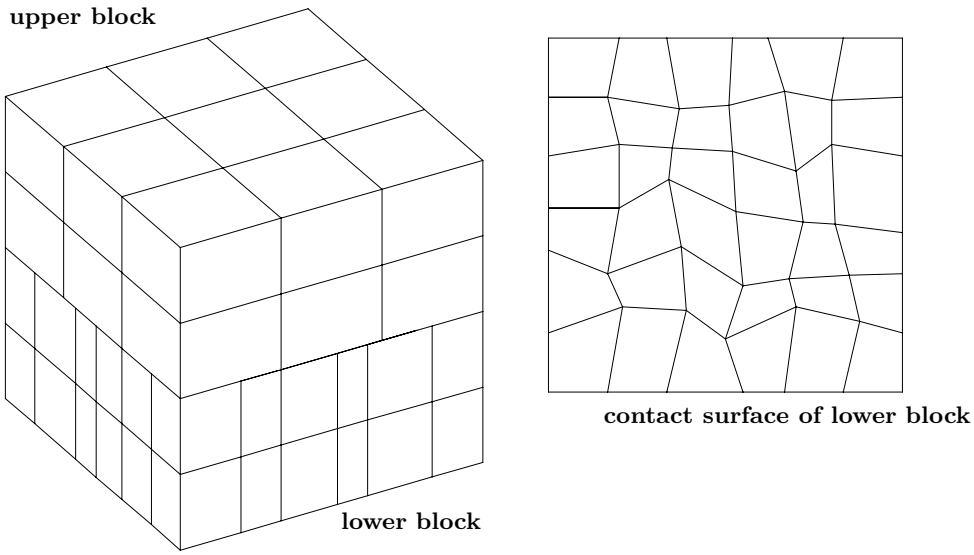

Figure 3: Blocks for the patch test in analogy to [13]. Upper block – regular mesh. Lower block – distorted mesh.

No. Gpt	**No. sbd.**	**tractions** N		**stress** σ_z		**displ.** u_z	
		$\bar{x} \cdot 10^4$	v %	$\bar{x} \cdot 10^3$	v %	$\bar{x} \cdot 10^{-2}$	v %
NTS^*	1	-1.3084	-68.087	-1.5248	-120.039	-0.9150	-157.93
2	1	-1.7767	-21.474	-4.6787	-2.5772	-2.4286	-7.7430
6	1	-1.6738	-19.851	-4.7077	-1.1663	-2.4143	-1.5571
3	2	-1.6210	-16.760	-4.7137	-0.8570	-2.4180	-1.2770
2	3	-1.6354	-17.331	-4.7115	-0.8789	-2.4170	-1.4131
10	1	-1.6614	-19.696	-4.7109	-0.8595	-2.4150	-1.3121
2	5	-1.6477	-15.793	-4.7113	-0.7798	-2.4166	-1.2097
5	2	-1.6408	-17.572	-4.7139	-0.7942	-2.4160	-1.2383
20	1	-1.6537	-19.226	-4.7124	-0.7791	-2.4164	-1.1597
10	2	-1.6408	-16.667	-4.7128	-0.7585	-2.4159	-1.1304
4	5	-1.6299	-16.790	-4.7141	-0.7136	-2.4158	-1.0822
5	4	-1.6447	-16.395	-4.7125	-0.7239	-2.4154	-1.1190
2	10	-1.6337	-16.341	-4.7126	-0.7578	-2.4170	-1.1335

Table 1: Patch test. Influence of different integration schemes. Mean value and coefficient of variation for the following quantities: contact tractions N on the contact surface, normal stresses σ_z in the lower block and vertical nodal displacements u_z on the contact surface. NTS^* - node-to-surface approach.

7.2 Free bending of a metal sheet on two cylinders

A second example is the free bending problem of a metal sheet (thickness $t = 0.25$) with an elasto-plastic material law with the following material data: $\kappa = 1.75 \cdot 10^4\ kN/cm^2$; $\mu = 8.077 \cdot 10^3\ kN/cm^2$; $y_0 = 16\ kN/cm^2$; $\varepsilon_p = 10\ kN/cm^3$, given in fig. 4.

At the beginning the metal sheet is positioned on two cylindrical rigid bodies (fig. 4). As loading a displacement u is prescribed in the center of the sheet. Due to symmetry only one half of the system has to be modeled and discretized using 12 bilinear resp. 6 biquadratic elements and a rather fine mesh with 100 bilinear resp. 50 biquadratic elements. The surface of the rigid cylinder is described analytically, the metal sheet is the "master" part. Fig. 5 contains the results for the computation of the overall force with bilinear elements for the metal sheet.

The Gauss integration formulae with 2×2, 3×3, 7×7 and 10×10 integration points are used and the results are compared with those obtained with a refined mesh of 100 elements, with 1 Gauss point only for non-frictional case. It is obvious, that the quadrature formulae with 2×2 integration points leads to rather large oscillations. A comparison with the frictional case for the following friction coefficients: $\mu = 0.1$, $\mu = 0.2$, $\mu = 0.3$ is presented in Fig. 6, where the computation was performed with the "best" 10×10 integration formula. As an obvious result, the reaction force is increasing following the modification of the friction coefficient.

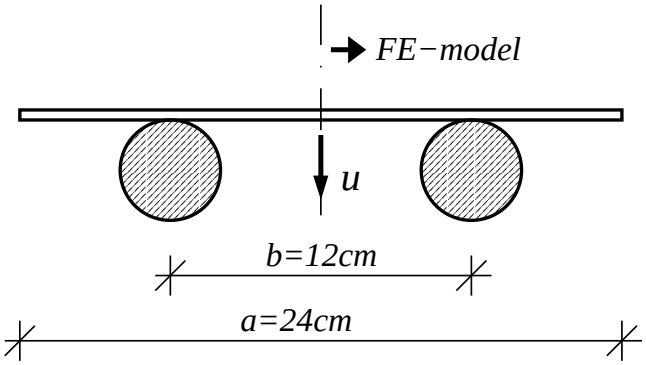

Figure 4: Geometry of free bending on two cylinders

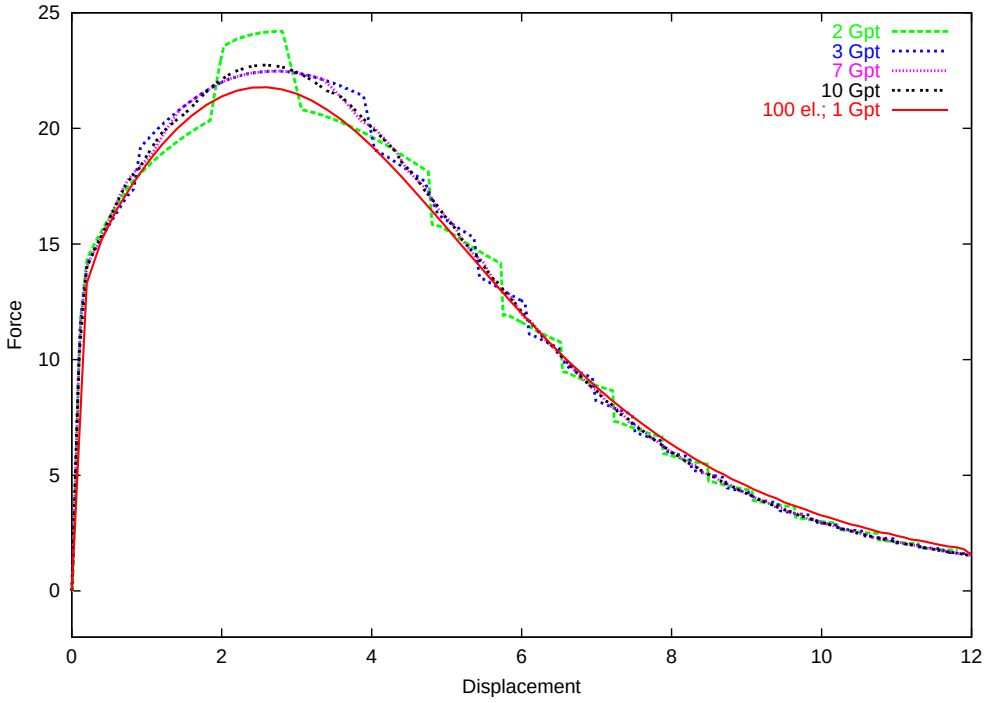

Figure 5: Force-deflection curves for free bending problem; bilinear elements; contact against analytically defined contact surface; influence of the number of Gauss points

The next step is to consider the influence of the number of Gauss points for the sheet meshed with biquadratic elements.

In fig. 7 the results of the computation for the beam meshed with 6 elements are given when **a)** the integration formula with 6×6 integration points and as an alternative **b)** the integration formula with 2 subdomains and 3×3 integration points in each and **c)** with

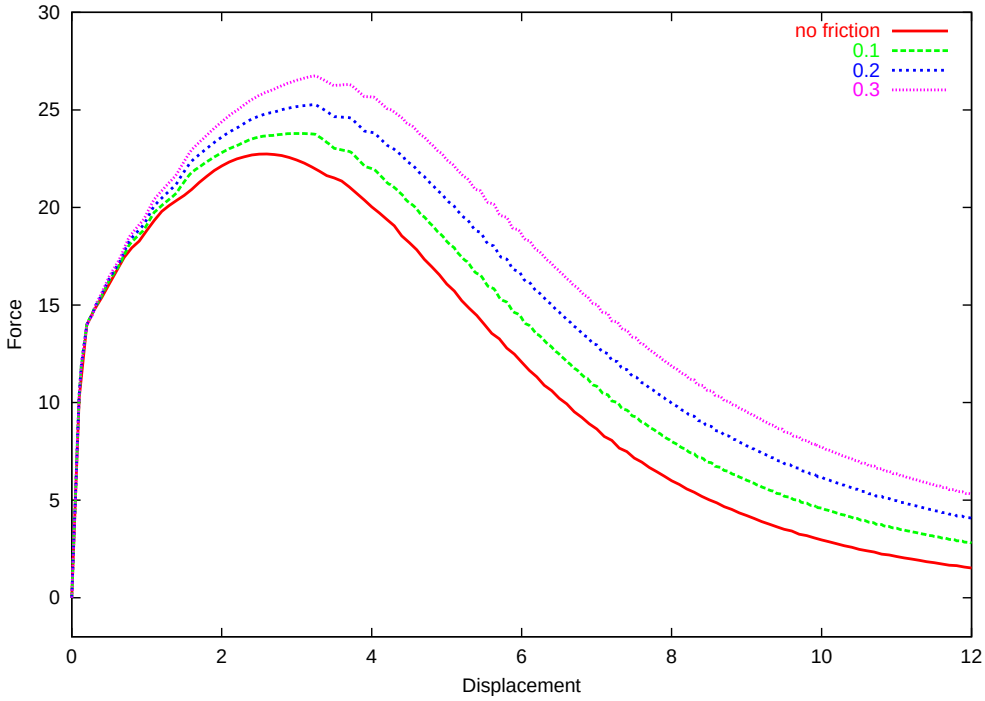

Figure 6: Force-deflection curves for free bending problem; influence of the choice for the friction coefficient; 10×10 Gauss points

3 subdomains and 2×2 integration points are used. The results are compared with those obtained with a refined mesh for the beam meshed with 12 elements and 3×3 integration points. For further comparison a 50 element mesh and 2×2 integration points per element is chosen. The density of the Gauss points to check the penetration is identical in the first three cases, but as a consequence of the smallest a-priori integration error for the algorithm with subdomains, the latter leads to the best reduction of the oscillations.

7.3 Deep drawing of a circular cylindrical part with a counter die

In this numerical example the deep drawing process of a cylindrical part with counter die is simulated, see the geometry in Fig. 8. The material of a circular plate is elasto-plastic with the following parameters: $\kappa = 1.75 \cdot 10^4\ kN/cm^2$; $\mu = 8077\ kN/cm^2$; $y_0 = 16\ kN/cm^2$.

The circular sheet has a uniform thickness $t = 1\ mm$ and a radius $R_S = 8\ cm$. The geometry of the tools is shown in fig. 8. Due to symmetry only a quarter of the structure is discretized using a mesh with 402 nodes. The contact surfaces of the rigid tools can be defined either as combination of plane surface, cylinder and torus, or as a surface of revolution, see sect. 6. As loading a displacement u is applied incrementally with $\Delta u = 0.0025$ for the punch, as well as for the counter die but for the latter after the punch is contacting the counter die. It can be seen from the deformation in Fig. 11 that the blank is dominantly drawn along the upper part of the die and the punch. The total force acting on the punch is computed as an integral over the contact area using the same number of integration points which were used for the contact integral and the tangent matrix. Fig. 9 contains the "total force-displacement" diagram for the punch computed for the following cases:
a) Non-frictional case. Integration: 5 Gauss points with 4 subdomains;
b) Frictional case with $\mu = 0.1$ and $\mu = 0.15$. Integration: 6 Gauss points.
Within the frictional analysis the contact between the punch and the sheet assumed to be

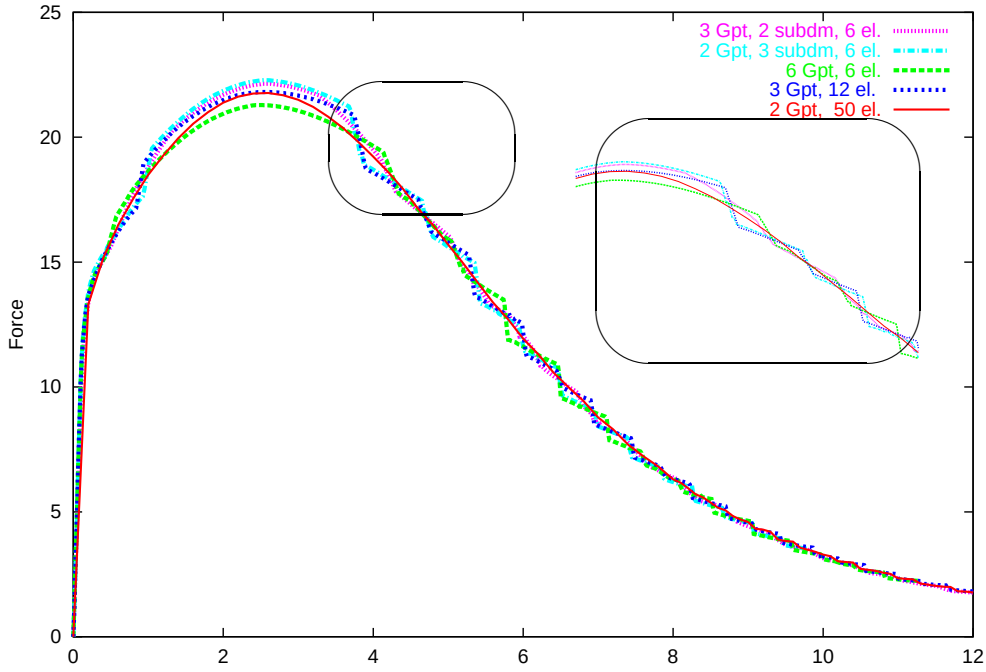

Figure 7: Force-deflection curves for free bending problem, bicubic elements; Influence of the number of Gauss points and refined mesh.

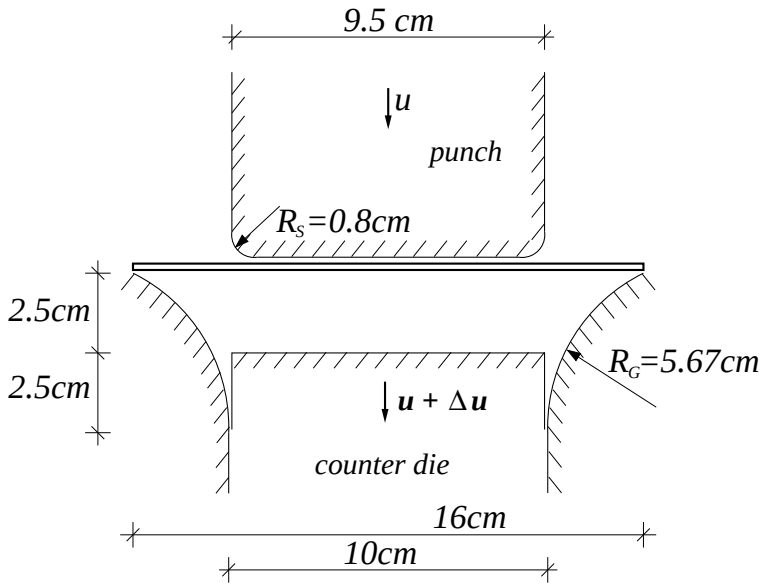

Figure 8: Geometry for deep drawing process

frictionless.

One of the advantages of the "solid-shell" formulation is ability to obtain the thickness strain, which can be crucial characteristics if the friction has been taken into account. Fig. 10 shows the thickness strain computed for the frictional case with the friction coefficient $\mu = 0.15$ at the point **A** with a radial coordinate $R = 4.8cm$, see diagram 11 d). As it can be seen from fig. 10, a frictional analysis gives twice as much of the strain thickness in comparison with the frictionless one.

8 CONCLUSIONS

- In the present contribution a fully covariant description of the contact condition and linearization in the case of Coulomb friction is proposed. A specially defined local coordinate system corresponding to the one used for closest point projection procedure was taken as a basis. All differential operations necessary for the linearization can be defined as covariant derivatives in that system.
- Several contact approaches are generalized under the unified description which leads to the segment-to-segment contact element and to the segment-to-analytical surface contact element. The last appears especially useful for applications in sheet metal forming where rigid tools can be commonly defined by arbitrarily smooth functions for the geometries. In this case the well-known closest point procedure can be turned into the computation of the value of penetration from the surface equations directly.
- An adaptive integration technique based on using subdomains is also proposed to overcome the problem of integration of a discontinuous function which appears during solution of the contact problem. It allows to considerably improve the characteristics in the contact patch test as well as to decrease oscillations of the force-deflection curves for relatively coarse meshes during the contact analysis.
- As an example of a realistic metal forming process a deep drawing of a sheet into a cylindrical pot is chosen. Here the ability of the 'Solid-Shells' to simulate complex forming processes with 3D effects with particular attention on the thickness strain together with the introduced contact formulations can be shown. The particular influence of friction on the some results characteristics is discussed.

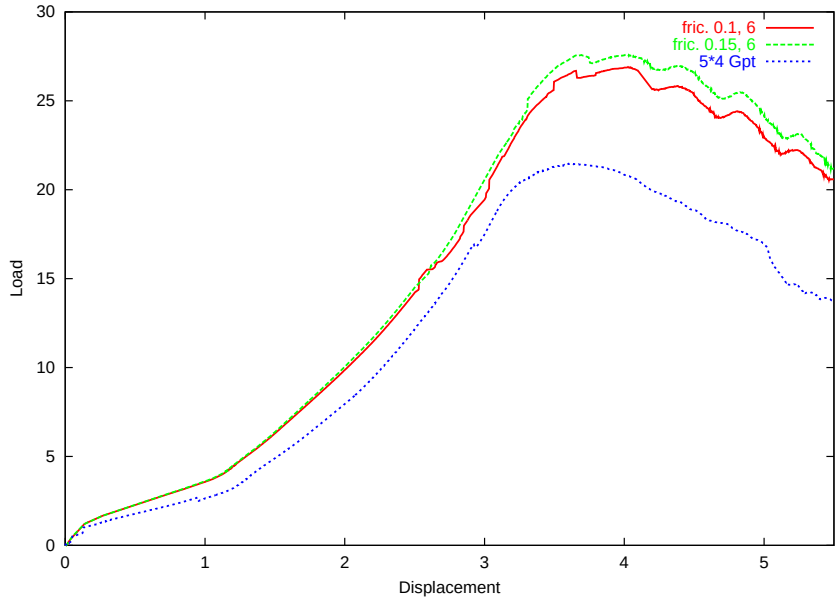

Figure 9: Deep drawing process. Total force vs. displacement for the punch with varying friction coefficient, compared to frictionless analysis with 4 subdomains and 5 Gauss points.

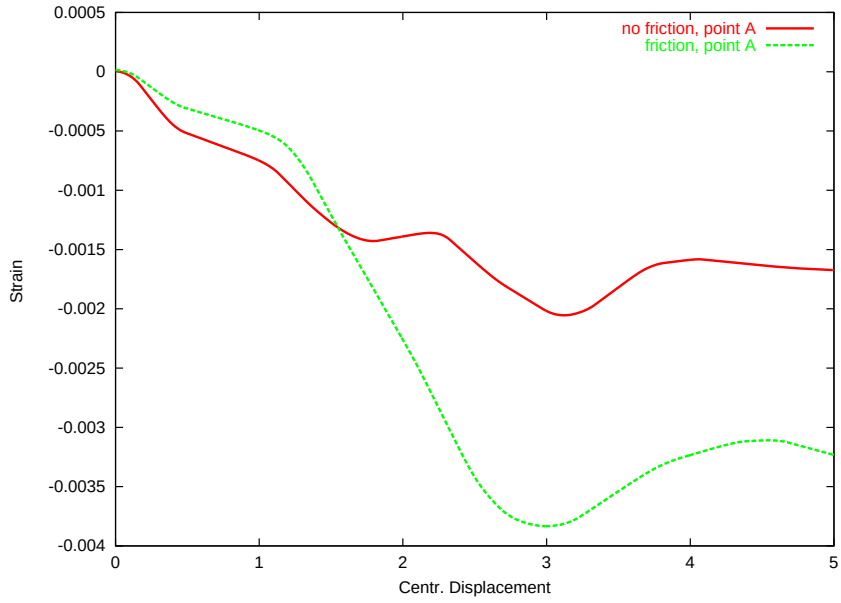

Figure 10: Deep drawing process. Thickness strain at point **A** vs. displacement of the central point. Comparing a frictionless analysis with a frictional case with $\mu = 0.15$

a) $u = 0.00\ cm$

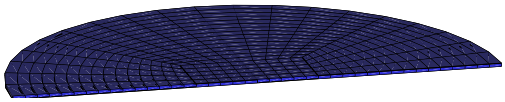

b) $u = 1.25\ cm$

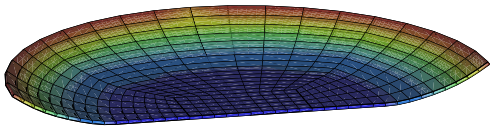

c) $u = 2.50\ cm$

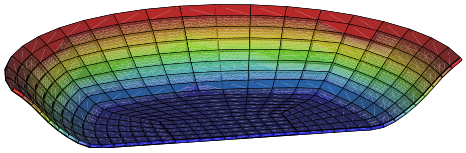

d) $u = 3.75\ cm$

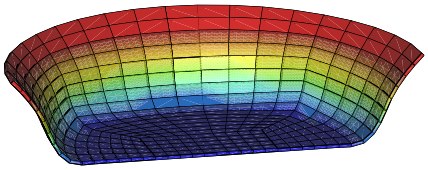

A: $R = 4.80\ cm$

d) $u = 5.00\ cm$

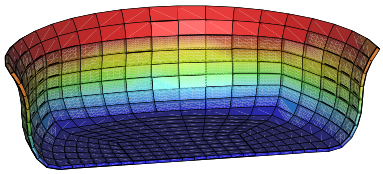

Figure 11: Deep drawing process. Blank at various deformation states for $\mu = 0$. Von Mises stresses for the sheet.

References

[1] P. Wriggers, Vu Van, E. Stein. Finite element formulation of large deformation impact-contact problem with friction. Comp. Struct., **vol. 37**, pp. 319-331, 1990.

[2] T. A. Laursen and J. C. Simo. A continuum-based finite element formulation for the implicit solution of multibody large deformation frictional contact problems. *Int. J. Numer. Methods Engng.*, **vol. 35**, pp. 3451-3485, 1993.

[3] H. Parisch and Ch. Lübbing. A formulation of arbitrarily shaped surface elements for three-dimensional large deformation contact with friction. *Int. J. Numer. Methods Engng.*, **40**, pp. 3359-3383, 1997.

[4] G. Pietrzak and A. Curnier. Large deformation frictional contact mechanics: continuum formulation and augmented Lagrangian treatment. *Comp. Meth. Appl. Mech. Engng.*, **vol. 177**, pp. 351-381, 1999.

[5] L. Krstulovic-Opara, P. Wriggers, J. Korelc. A C^1-continuous formulation for 3D finite deformation frictional contact. *Comput. Mech.*, **vol. 29**, pp. 27-42, 2002.

[6] M. A. Puso and T. A. Laursen. A 3D contact smoothing method using Gregory patches. *Int. J. Numer. Methods Engng.*, **vol. 54**, pp. 1161-1194, 2002.

[7] R. Hauptmann and K. Schweizerhof. A systematic development of solid-shell element formulations for linear and nonlinear analyses employing only displacement degrees of freedom. *Int. J. Numer. Methods Engng.*, **vol. 42**, 49–70, 1998.

[8] R. Hauptmann, S. Doll, M. Harnau, K. Schweizerhof. 'Solid-Shell' elements with linear and quadratic shape functions at large deformations with nearly incompressible materials. *Comp. Struct.*, **vol. 79**, 1671–1685, 2001.

[9] A. Konyukhov and K. Schweizerhof. Contact formulation via a velocity description allowing efficiency improvements in frictionless contact analysis. *Comput. Mech.*, **vol. 33**, 165–173, 2003.

[10] P. Wriggers. *Computational Contact Mechanics.* John Wiley & Sons, 2002.

[11] T. A. Laursen. *Computational Contact and Impact Mechanics.* Springer, 2002.

[12] P. J. Davis and P. Rabinowitz. *Methods of numerical integration.* Academic Press, 1984.

[13] M.A. Crisfield. Re-visiting the contact patch test. *Int. J. Numer. Methods Engng.*, 48:435-449, 2000.